Delta-Sigma Digitization and Optical Coherent Transmission of DOCSIS 3.1 Signals in Hybrid Fiber Coax Networks

Jing Wang, Zhensheng Jia, Luis Alberto Campos, Lin Cheng, Curtis Knittle, and Gee-Kung Chang, *Fellow, IEEE, Fellow, OSA*

(Top-Scored Paper)

***Abstract*—We first demonstrate delta-sigma digitization and coherent transmission of data over cable system interface specification (DOCSIS) 3.1 signals in a hybrid fiber coax (HFC) network. Twenty 192-MHz DOCSIS 3.1 channels with modulation up to 16384QAM are digitized by a low-pass cascade resonator feedback (CRFB) delta-sigma analog-to-digital converter (ADC) and transmitted over 80-km fiber using coherent single-λ 128-Gb/s dual-polarization (DP) quadrature phase-shift keying (QPSK) and 256-Gb/s DP-16QAM optical links. Both one-bit and two-bit delta-sigma digitization are implemented and supported by the QPSK and 16QAM coherent transmission systems, respectively. To facilitate its practical application in access networks, the coherent system is built using a low-cost narrow-band optical modulator and RF amplifiers. Modulation error ratio (MER) larger than 50 dB is successfully demonstrated for all 20 DOCSIS 3.1 channels, and high-order modulation up to 16384QAM is delivered over fiber for the first time in HFC networks. The raw DOCSIS data capacity is 54 Gb/s with net user information ∼45 Gb/s. Moreover, the bit error ratio (BER) tolerance is evaluated by measuring the MER performance as BER increases. Negligible MER degradation is observed for BER up to 1.5×10^{-6} and 1.7×10^{-4} for one-bit and two-bit digitization, respectively.**

***Index Terms*—Access network, delta-sigma ADC, digitization, DOCSIS 3.1, hybrid fiber coax, OFDM.**

I. Introduction

VIDEO-INTENSIVE services, such as virtual reality and immersive applications are driving the growth of data traffic at user premises in an explosive way, making access networks become a bottleneck of user quality of experience. Various optical and wireless access technologies have been investigated, including passive optical networks (PON) [1]–[3], cloud-radio access networks (C-RAN) [4]–[7], and hybrid fiber coax (HFC) networks [8], [9]. In the United States, there are more than 50 million subscribers using cable services for broadband access, which is 40% more than digital subscriber line (DSL) and fiber-to-the-home (FTTH) users [10]. Given the emergence of data over cable service interface specification (DOCSIS) 3.1, it is expected that HFC networks will continue to dominate the broadband access market in the United States, delivering fastest access speed to the broadest population.

As a fifth-generation broadband access technology, DOCSIS 3.1 specifications are being commercialized at a historically rapid pace to support ultra-high resolution videos (4 K/8 K), mobile backhaul/fronthaul (MBH/MFH), and other emerging applications enabled by virtual reality and internet of things [10]–[14]. DOCSIS 3.1 specifications involve enhancement in both physical and MAC layers, which transform the physical layer signal from single-carrier QAM (SC-QAM) to orthogonal frequency division multiplexing (OFDM), for increased data rate, improved spectral efficiency, and flexible resource allocation. It provides up to 10 Gb/s downstream and 1.8 Gb/s upstream capacities to each subscriber [15], [16]. With subcarrier spacing of 25 or 50 kHz, DOCSIS 3.1 specifications support downstream channel of 24–192 MHz, and upstream channel of 6.4–96 MHz [17]–[19]. Moreover, higher order modulations up to 4096QAM were adopted with optional support of 8192 and 16384QAM [10], [15]. Similar to LTE carrier aggregation in MFH networks [20], [21], DOCSIS 3.1 specifications support channel bonding to designate more than one DOCSIS channels to a single user.

The continuous envelope and high peak-to-average power ratio (PAPR) of OFDM signals, on the other hand, make them vulnerable to noise and nonlinear impairments in analog HFC networks [22]–[24]. Combined with demanding carrier-to-noise ratio (CNR) requirements of high order modulations (>4096QAM), it is difficult to support DOCSIS 3.1 signals by legacy analog fiber links [15]. In this paper, for the first time we demonstrate the digitization of DOCSIS 3.1 signals to enable the upgrade of fiber distribution networks from analog to digital, so mature digital fiber technologies, e.g., intensity mod-

Manuscript received June 30, 2017; revised October 25, 2017; accepted November 17, 2017. Date of publication November 19, 2017; date of current version February 24, 2018. This work was supported in part by Cable Television Laboratories, Inc., and the NSF Center of Fiber-Wireless Integration and Networking. *(Corresponding author: Jing Wang.)*

J. Wang and L. Cheng were with Georgia Institute of Technology, Atlanta, GA 30308 USA. They are now with Cable Television Laboratories, Inc., Louisville, CO 80027 USA (e-mail: j.wang@cablelabs.com; l.cheng@cablelabs.com).

Z. Jia, L. A. Campos, and C. Knittle are with Cable Television Laboratories, Inc, Louisville, CO 80027 USA (e-mail: s.jia@cablelabs.com; a.campos@cablelabs.com; c.knittle@cablelabs.com).

G.-K. Chang is with Georgia Institute of Technology, Atlanta, GA 30308 USA (e-mail: geekung.chang@ece.gatech.edu).

Color versions of one or more of the figures in this paper are available online at http://ieeexplore.ieee.org.

Digital Object Identifier 10.1109/JLT.2017.2775858

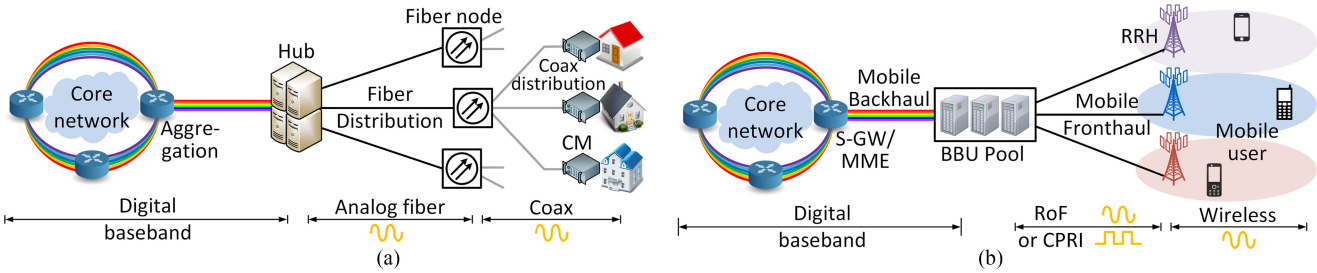

Fig. 1. Architecture of HFC network and C-RAN. (a) HFC network. (b) C-RAN.

ulation/direct detection (IM/DD) and coherent optical transmission, can be exploited.

To enable digital transmission of DOCSIS 3.1 signals, a digitization interface, i.e., analog-to-digital converter (ADC), is needed in the hub to digitize the analog signals into bits, and a digital-to-analog converter (DAC) is needed in the fiber node to retrieve the analog waveforms from digital bits for the following transmission over coaxial cable plant. Different from conventional Nyquist AD/DA that uses Nyquist sampling rates, such as common public radio interface (CPRI) in MFH networks [25], which has quantization noise evenly distributed in the frequency domain and needs many quantization bits, delta-sigma ADC features high sampling rate but only a few (one or two) quantization bits, and most importantly, it utilizes a noise shaping technique to push the quantization noise out of the signal band, so that signal and noise are separated in the frequency domain, and the in-band CNR of the digitized signal can be optimized [26]–[29]. Moreover, delta-sigma digitization enables a simplified DAC design based on low-cost passive filters in the fiber node, which filters out the desired signals, eliminates the out-of-band noise, and at the same time, retrieves the analog waveforms. In the hub, a high speed delta-sigma ADC is shared by multiple fiber nodes; whereas in each fiber node, only a low-cost passive filter is needed to filter out the desired signal and convert it to the analog waveform. Since there are more fiber nodes than hubs, especially given the fact that fiber node number is continuing to grow due to node segmentation and fiber deep migration, replacing Nyquist DAC with a low-cost passive filter can significantly reduce the cost and complexity of fiber nodes.

Delta-sigma digitization has found wide applications in power amplifiers [30]–[32], RF transmitters [33]–[37] and receivers [38]–[42], visible light communications [43], [44], radio-over-fiber (RoF) [45]–[47], and MFH networks [48]–[50]. In Ref. [48]–[50], we first demonstrated delta-sigma digitization as a new digitization interface in MHF networks to replace CPRI, and 32 LTE carrier aggregation was demonstrated within a single-λ 10-Gb/s PON system to support 3GPP release 13. We then extended delta-sigma digitization to DOCSIS signals for HFC networks [51]. This paper is an extended version of our previous work [51] with substantial details and new results.

In this paper, we for the first time demonstrate the delta-sigma digitization of twenty 192-MHz DOCSIS 3.1 channels with 16384QAM modulation, based on a low-pass cascade resonator feedback (CRFB) delta-sigma ADC. We transmit the digitized bits over 80-km fiber by a low-cost single-λ 128-Gb/s dual-polarization (DP)-QPSK or 256-Gb/s DP-16QAM coherent fiber link. Both one-bit and two-bit delta-sigma digitization are realized and supported by the coherent QPSK/16QAM links, respectively. To facilitate its application in access networks, the coherent fiber link is built using low-cost narrowband RF amplifiers and optical modulator. More than 50-dB modulation error ratio (MER) is achieved for all 20 DOCSIS 3.1 channels, and high order modulation up to 16384QAM is demonstrated and delivered over fiber for the first time in HFC networks. The raw DOCSIS data rate is 54 Gb/s with net user information $\sim$45 Gb/s. The bit error ratio (BER) tolerance of delta-sigma digitization is also evaluated and negligible MER performance degradation is observed for BER values up to 1.5×10^{-6} and 1.7×10^{-4}, for one-bit and two-bit digitization, respectively.

This paper is organized as follows. Section II discusses the operation principles of delta-sigma digitization. Section III presents the experimental setup. Section IV shows the design of delta-sigma ADC. The experimental results are shown in Section V. Section V concludes the paper.

II. Operation Principles

The architecture of a HFC network is shown in Fig. 1. Due to their similarity, a C-RAN architecture is also presented for comparison. In Fig. 1(b), the network segment from service gateway (S-GW) or mobile management entity (MME) to baseband unit (BBU) is defined as mobile backhaul (MBH), which transmits the control and payload bits of LTE signals in digital baseband. The digital bits are received by BBUs, which synthesizes OFDM modulation and generates analog waveform of LTE signals. The network segment from BBU to remote radio heads (RRH) is defined as mobile fronthaul (MFH), where the LTE signals are transmitted over fiber in either analog waveform using RoF technology or digital waveform via CPRI digitization interface. The last segment of C-RAN involves the wireless transmission from the RRHs to mobile users, where LTE signals are transmitted in their analog waveforms via air interface.

Similarly, HFC networks in Fig. 1(a) can also be divided into three segments, i.e., the core network segment from the aggregation node to the hub, the fiber distribution network from hub to fiber nodes, and the coaxial cable plant from fiber nodes to cable modems (CMs). Similar to MBH, the segment from the aggregation node to hub transmits net bit information; similar to MFH, the fiber distribution segment from hub to fiber node is supported by either analog or digital fiber technologies, e.g., C-RAN uses RoF technology to deliver analog mobile signals; HFC uses analog fiber links to deliver analog DOCSIS/video

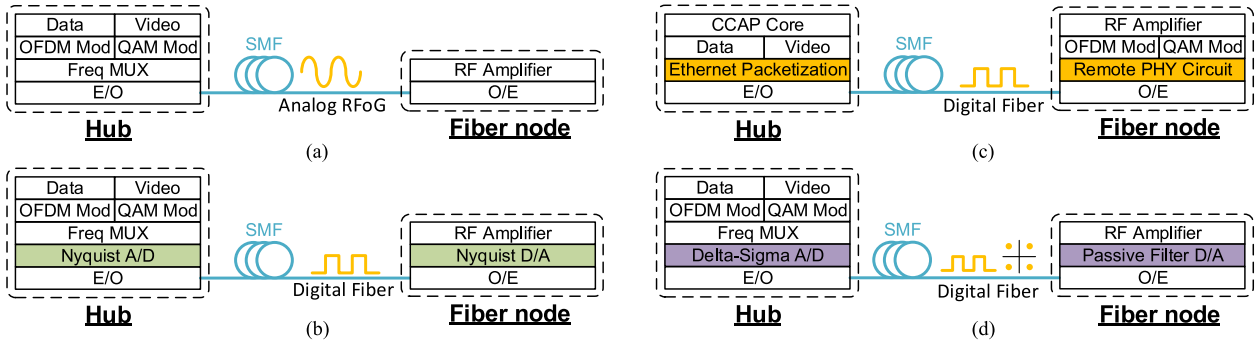

Fig. 2. Different analog/digital technologies for fiber distribution network. (a) Analog fiber link. (b) Digital fiber link based on BDF/BDR. (c) Digital fiber link based on remote PHY. (d) Digital fiber link based on delta-sigma digitization.

signals; C-RAN uses CPRI as a Nyquist digitization interface; HFC has a similar interface called baseband digital forward or return (BDF/BDR). The last segment of HFC network from fiber node to CMs is also similar to the wireless segment of C-RAN, where both DOCSIS and LTE signals are transmitted in the analog waveform over coaxial cable or air interface. Different analog or digital implementations of the fiber distribution network segment are shown in Fig. 2.

A. Analog Fiber

Fig. 2(a) shows the architecture of an analog fiber link. DOCSIS and video signals are aggregated in the hub/headend and delivered to the fiber node in analog waveforms. Then at the fiber node, the received analog signals are delivered to CMs via cable distribution networks. An analog fiber link features simple, low-cost implementation, and high spectral efficiency, but imposes high linearity requirements on the channel response. Since it does not perform any data reformation, an analog fiber link is a waveform/service agnostic pipe, and can be used for various services, e.g., DOCSIS, MPEG, and analog TV. On the other hand, it suffers from noise and nonlinear impairments, limited signal-to-noise ratio (SNR), short fiber distance, and small number of WDM wavelengths. It also requires complex RF amplifiers and bi-annual calibration of fiber nodes.

B. BDF/BDR

Upgrading fiber distribution networks from analog to digital offers the opportunity to leverage the mature digital fiber access technologies. Due to the wide deployment of Ethernet, digital fiber link features low cost, high capacity, long transmission distance, and easy setup and maintenance, as compared with its analog counterpart. Moreover, the contribution of optical noise and nonlinear impairments can be isolated from the received signal quality, so large SNR and high order modulation can be achieved. Since it can support many (>80) WDM wavelengths, digital fiber link facilitates the fiber deep and node segmentation migrations. Fig. 2(b)–(d) show three different digital fiber technologies.

Fig. 2(b) shows a digital fiber link based on BDF/BDR architecture, where a Nyquist ADC is inserted in the hub with 2.5 oversampling ratio and 12 quantization bits. At fiber node, a Nyquist DAC retrieves the analog signals, and feeds them to the coaxial cable plant. Same as CPRI, BDF/BDR provides a simple, low-cost, and service-transparent digitization interface, but with the penalty of low spectral efficiency. Similar to CPRI, the digitized bits of BDF/BDR are not encapsulated into Ethernet packets but framed by time-division-multiplexing (TDM), so it always runs at the full data rate even without any real payload. This makes traffic engineering based on statistical multiplexing impossible. In today's HFC networks, there is only upstream BDR deployed, but no downstream BDF, and the BDR specifications are vendor proprietary and not interoperable.

C. Remote PHY

Digital fiber link based on remote PHY architecture is shown in Fig. 2(c), where the PHY chips for OFDM/QAM modulation and demodulation are moved to the fiber node, and an integrated converged cable access platform (CCAP) is separated into a CCAP core in the hub and a remote PHY device (RPD) in the fiber node [52]–[56]. In the downstream, payload and control bits are packetized into Ethernet packets and transmitted from the hub to the fiber node, where the OFDM/QAM modulators synthesize analog DOCSIS/MPEG signals for cable distribution. In the upstream, OFDM/QAM demodulators interpret the received analog signals into baseband bits, and transmit them back to the hub in Ethernet packets. Compared with analog fiber link in Fig. 2(a), the RF interface in hub is replaced by an Ethernet interface, and in fiber node, there is an Ethernet interface connecting to the digital fiber and a RF interface connecting to the coaxial cable plant. With the help of Ethernet packetization, remote PHY architecture can exploit Ethernet access technologies, such as Ethernet PON (EPON), gigabit PON (GPON), and Metro Ethernet [52]–[54], and enable statistical multiplexing for traffic engineering. Compared with other digital solutions, remote PHY features smaller traffic load in the fiber, but with the penalty of increased complexity and cost of fiber nodes. Due to the modulation/demodulation at RPD, the fiber link in remote PHY architecture is no longer a service-transparent pipe, although it maintains the least amount of hardware exported to RPD, and preserves the compatibility with existing hubs in analog fiber links. It should be noted that the concepts of remote PHY/MAC are very similar to the function split of MFH networks [57]–[59], by moving partial physical and/or MAC layer functions from the centralized entity (hub/BBU) to remote nodes (fiber node/RRH).

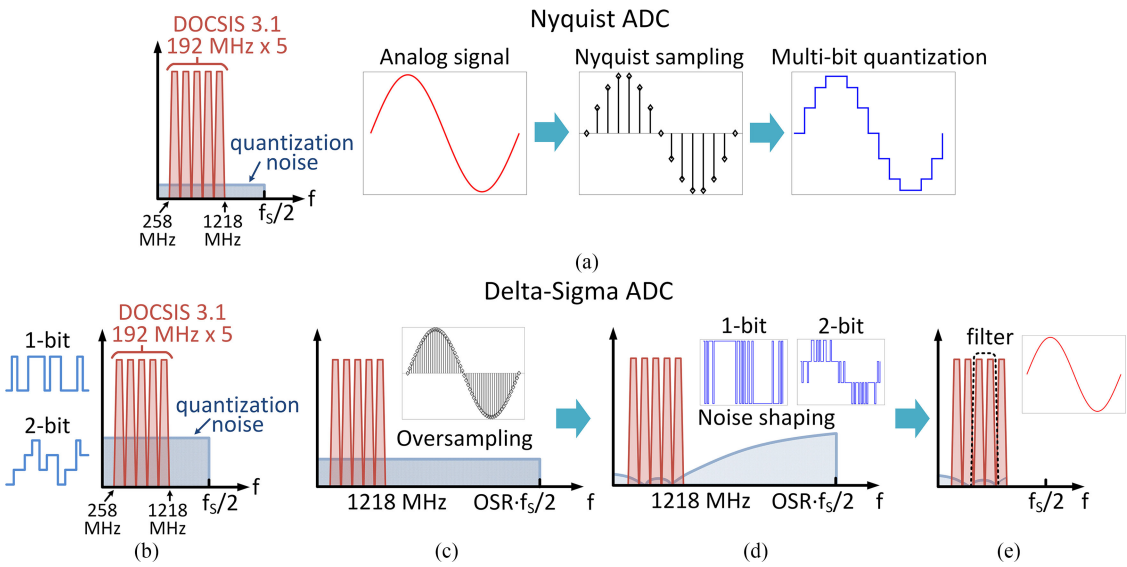

Fig. 3. Operation principle of Nyquist ADC and delta-sigma ADC. (a) Nyquist ADC samples analog signals at Nyquist rate, and each sample is quantized by multiple quantization bits. BDF/BDR uses a Nyquist ADC. (b) Since delta-sigma ADC only uses one or two quantization bits, it cannot run at Nyquist sampling rate, otherwise significant quantization noise will be introduced. (c) Delta-sigma ADC uses oversampling to extend the Nyquist zone, so the quantization noise is spread over a wide frequency range. (d) Noise transfer function shapes the distribution of quantization noise, and pushes it out of the signal band. So the signal and noise are separated in the frequency domain. (e) In CM, analog signals can be retrieved by passive filtering which eliminates the out-of-band quantization noise.

D. delta-sigma Digitization

Fig. 2(d) shows the architecture of delta-sigma digitization. Compared with Fig. 2(b), Nyquist AD/DA in BDF/BDR are replaced by a delta-sigma ADC in hub and a passive filter in fiber node. Different from the Nyquist ADC with oversampling ratio of 2.5 and 12 quantization bits, delta-sigma ADC trades quantization bits for sampling rate, using high sampling rate but only a few (one or two) quantization bits. Its operation principle is shown in Fig. 3. For reference, the operation principle of Nyquist ADC is also presented in Fig. 3(a). In this paper, we designed a delta-sigma ADC to digitize five DOCSIS 3.1 channels with channel bandwidth of 192 MHz and total frequency range from 258 MHz to 1218 MHz ($5 \times 192 = 960$ MHz). Due to the limited quantization bits, Nyquist sampling rate would lead to significant quantization noise (Fig. 3(b)). Oversampling is utilized to extend the Nyquist zone and spread the quantization noise over a wide frequency range, so the in-band noise is reduced (Fig. 3(c)).

Furthermore, noise shaping technique is used to push the quantization noise out of the signal band, which acts as a high-pass filter (HPF) to the quantization noise and separates the signal and noise in the frequency domain, as shown in Fig. 3(d). It should be noted that during the delta-sigma digitization, the signal spectrum is kept intact; it is the out-of-band quantization noise added by the delta-sigma ADC that converts the signal waveform from analog to digital. Therefore, in Fig. 3(e) at the receiver side, when the out-of-band quantization noise is eliminated, the signal waveform will be automatically converted back from digital to analog, i.e., a passive filter not only filters out the desired signal channel, but also realizes the digital-to-analog conversion. In HFC networks, a high speed delta-sigma ADC is centralized in the hub and shared by many fiber nodes, and each fiber node only needs a low-cost passive filter to select the desired DOCSIS channels and at the same time convert them to the analog waveform. This design reduces the cost and complexity of fiber nodes. Given the fact that there are many more fiber nodes than hubs/headends, the overall system cost is significantly reduced. It should be note that Nyquist ADC has quantization noise evenly distributed in the frequency domain; whereas delta-sigma digitization has a shaped distribution of quantization noise, so the retrieved analog signal has an uneven noise floor.

In time domain, if we use an analog sinusoidal signal as an example, a Nyquist ADC samples the analog input with Nyquist rate and each sample is quantized individually (Fig. 3(a)); whereas delta-sigma ADC samples the analog input at a much higher rate and the samples are digitized consecutively (Fig. 3(c) and (d)), i.e., the current digitization bits not only depend on the current analog input, but also depend on previous input. One-bit delta-sigma digitization outputs a high data rate on-off keying (OOK) signal with the density of "1" bits being proportional to the amplitude of analog input. For maximum input, it outputs continuous "1"s; for minimum input, it outputs continuous "0"s. For intermediate inputs, the densities of "0"s and "1"s are almost equal. Two-bit digitization outputs a 4-level pulse-amplitude-modulation (PAM4) signal. Both one-bit and two-bit digitization are implemented in our experiment.

Table I compares different analog/digital fiber technologies in HFC networks. As a waveform-agnostic interface, delta-sigma ADC works with not only OFDM signals but also 5G multi-carrier waveforms, such as filter-band multicarrier signals, as we reported in [50]. Analog fiber, BDF/BDR, and delta-sigma digitization are service-agnostic and can carry a combination of different services, even though these services evolve in the future. Remote PHY, on the other hand, is not service-transparent.

TABLE I
COMPARISON OF ANALOG/DIGITAL FIBER TECHNOLOGIES IN HFC NETWORKS

	Analog	Digital		
Interface	Linear optics	BDF/BDR	Remote PHY	Delta-sigma digitization
Operation principles	Analog RF over fiber	Nyquist AD/DA in hub and fiber node	Move PHY circuits of OFDM/QAM modulation/demodulation to fiber node Transmit net information bits over fiber	Delta-sigma ADC in hub Passive filter in fiber node as DAC
AD/DA	N/A	2.5 oversampling ratio 12 quantization bits	N/A	High sampling rate 1-2 quantization bits
Pros	Simple implementation High spectral efficiency Waveform/service agnostic	High capacity, Large SNR, High order modulation, Long distance, Scalability, Easy setup and maintenance, Many WDM wavelengths, Facilitate node split and fiber deep migration		
		No modification of bits Waveform/service agnostic Simple, low-cost AD/DA	Ethernet packet encapsulation Statistical multiplexing Reduced fiber traffic load	No modification of bits Waveform/service agnostic Low-cost DA based on passive filters
Cons	Short distance Small capacity SNR limited by noise/nonlinearities Few WDM wavelengths	Low spectral efficiency No Ethernet encapsulation Always run at full data rate Vendor proprietary	Modification of bits Not transparent to waveform/service Increased complexity/cost of fiber nodes	High cost delta-sigma ADC

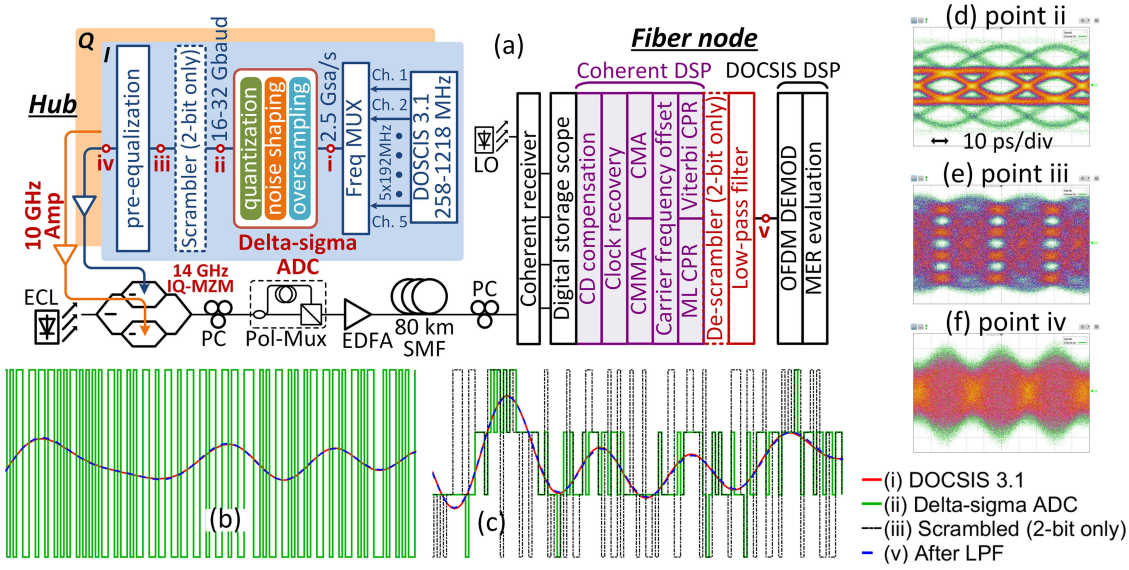

Fig. 4. (a) Experimental setup. (b) Waveforms for one-bit delta-sigma digitization. (c) Waveforms for two-bit delta-sigma digitization. (d) Eye diagram of 32 Gbaud PAM4 signal after delta-sigma ADC (point ii). (e) PAM4 eye diagram after the scrambler (point iii). (f) PAM4 eye diagram after pre-equalization (point iv).

TABLE II
OFDM PARAMETERS OF DOCSIS 3.1 SIGNALS

Sampling rate	FFT size	Subcarrier spacing	Active subcarriers	Active BW	Data subcarriers	Data BW	Guard band
204.8 MSa/s	4096*	50 kHz	3840	192 MHz	3800	190 MHz	1 MHz
	8192	25 kHz	7680		7600		

* In experiments, we use FFT size of 4096 and subcarrier spacing of 50 kHz.

Its RPD in the fiber node is only designed for one specific service.

III. EXPERIMENTAL SETUP

Fig. 4 shows the experimental setup. OFDM parameters of DOCSIS 3.1 specifications are listed in Table II. There are two sets of FFT sizes and subcarrier spacing. In this experiments, we use the FFT size of 4096 and subcarrier spacing of 50 kHz.

In a 1.2 GHz DOCSIS 3.1 implementation, the downstream signal contains five channels, each with 192-MHz bandwidth and occupying 960-MHz (258-1218 MHz) frequency band in total. In this experiment, these five downstream channels are digitized by delta-sigma ADCs with sampling rates of 16, 20, 24, 28, and 32 GSa/s. Both one-bit and two-bit digitization are carried out, and the five channels are digitized to an OOK (one-bit) or PAM4 (two-bit) signal with baud rate of 16-32 Gbaud. In a dual-polarization (DP) coherent fiber link, each polarization has in-phase (I) and quadrature (Q) components, and each component can carry one OOK/PAM4 signal, so there are four data streams in total carrying 20 digitized DOCSIS 3.1 channels, i.e., a DP-QPSK link carries 20 digitized DOCSIS channels with

TABLE III
CARRIER-TO-NOISE RATIO (CNR) REQUIREMENTS IN DOCSIS 3.1 SPECIFICATIONS FOR DIFFERENT MODULATION ORDERS

QAM	16	64	128	256	512	1024	2048	4096	8192*	16384*
CNR (dB)	15	21	24	27	30.5	34	37 (37.5)$^+$	41 (41.5)$^+$	44 (44.5)$^+$	48 (48.5)$^+$

* For DOCSIS 3.1 downstream, 8192QAM and 16384QAM are optional, and their CNRs are not specified yet. Here we use 44(44.5) and 48(48.5) dB as temporary criteria.
$^+$ CNR values in parentheses with 0.5-dB increment are for channels above 1 GHz.

four streams of OOK signals. Delivering 20 DOCSIS channels over a single wavelength quadruples the capacity of current HFC networks and enables a 4x1 fiber node segmentation. In the following sections, only the results of 32 Gbaud are discussed in detail due to the limited space.

In Fig. 4, the two arms of the IQ Mach-Zehnder modulator (MZM) are driven by two independent OOK/PAM4 signals to synthesize a QPSK/16QAM signal, and after the polarization multiplexer, a DP-QPSK/16QAM signal carries four streams of OOK/PAM4 with totally 20 digitized DOCSIS channels.

It is worth noting that although there are several reports of high speed delta-sigma ADC with sampling rate up to 8.6 GSa/s [35]–[37], there is no commercially available delta-sigma ADC that runs faster than 10 GSa/s. For a proof-of-concept experiment in this paper, the delta-sigma digitization is realized offline using MATLAB, and the digitized bits are loaded into a Keysight arbitrary waveform generator (AWG) M8196A, and then transmitted over a 80-km coherent fiber link. In real implementations, to alleviate the speed limit, several low speed delta-sigma ADCs can be used in parallel, each digitizing only one DOCSIS channel, rather than using a high speed ADC to digitize all five channels together. The output bits from several parallel low speed ADCs can be interleaved in the time domain by TDM technology, so the sampling rate of each ADC is reduced, while the overall capacity is kept intact.

In Fig. 4(b) and (c), analog DOCSIS 3.1 signal at point i is plotted in red; after delta-sigma digitization, the OOK/PAM4 signals at point ii are plot in green; the retrieved analog signals after filters at point v are plotted in dashed blue lines. The initial (red) and retrieved (dashed blue) analog signals are fairly close to each other, indicating that the digitization introduces almost no impairment. In the green curve of Fig. 4(c), there are more ± 1 symbols than ± 3 symbols. This is because DOCSIS 3.1 is an OFDM signal with Gaussian distribution, and there are much more small samples than large ones. So the PAM4 signal after digitization also has unequal distribution. More than 80% symbols are ± 1s, and only less than 20% are ± 3s. This also makes the 16QAM signal has unequal distribution on its constellation. Most symbols are at (± 1 $\pm$j), and only a few at (± 3 ± 3j). Unequally distributed constellation introduces challenges to the digital signal processing (DSP) of the coherent receiver, especially for constant multiple modulus algorithm (CMMA). To equalize the symbol distribution, a scrambler is inserted in the transmitter (only for two-bit digitization). Eye diagrams before and after the scrambler are shown in Fig. 4(d) and (e). In Fig. 4(d), there are much more ± 1s than ± 3s; in Fig. 4(e), the amount of ± 1s and ± 3s are equalized.

Since delta-sigma digitization is designed to be utilized in access networks, such as HFC and C-RAN, a low-cost coherent system was built based on narrowband devices, e.g., 10 GHz RF drivers (Picosecond Pulse Labs 5822B) and 14 GHz IQ-MZM (Covega LN86S-FC). For 32 Gbaud QPSK/16QAM, these narrowband devices significantly impair the transmission performance, and frequency domain pre-equalization was used to compensate the bandwidth limitation. Fig. 4(f) shows the 32 Gbaud PAM4 eye diagram after pre-equalization. The eye is closed due to the boosted high frequency components.

After 80-km single mode fiber, the DP-QPSK/16QAM signal is received at the fiber node. In experiments, a Keysight N4391A optical modulation analyzer is used as a polarization diversity receiver. Four received signals (two polarizations, each polarization has in-phase and quadrature components) are captured by a real-time digital storage oscilloscope Keysight DSAX92004A for offline DSP. We use standard coherent DSP algorithms, including Gram-Schmidt orthogonalization [60], chromatic dispersion (CD) compensation [61], [62], polarization de-multiplexing [63], [64], carrier frequency offset (CFO) recovery [65], [66], and carrier phase recovery (CPR) [67], [68]. For polarization de-multiplexing, QPSK uses constant modulus algorithm (CMA), 16QAM uses constant multiple modulus algorithm (CMMA). For CPR, QPSK uses Viterbi-Viterbi algorithm, 16QAM uses the maximum likelihood (ML) phase recovery algorithm. After coherent DSP, a de-scrambler is applied to the PAM4 signal to restore its initial symbol distribution, and five DOCSIS channels are filtered out by a digital filter to retrieve their analog waveforms.

To evaluate the performance of delta-sigma digitization and coherent transmission, we use carrier-to-noise ratio (CNR) of received DOCSIS channels as a measurement. Required CNR for different modulations in DOCSIS 3.1 specifications are listed in Table III [15]. Higher order modulations need higher CNR, and there is 0.5-dB increment for the fifth channel above 1 GHz (1026-1218 MHz). The maximum mandatory modulation in DOCSIS 3.1 specification is 4096QAM. 8192 and 16384QAM are optional, and their CNR requirements are not specified yet. Here we use 44 dB and 48 dB based on extrapolation. In experiments, CNR is evaluated in terms of modulation error ratio (MER).

IV. EXPERIMENTAL DESIGN

In this section, we first present the design of delta-sigma ADC and discuss the experimental design, then demonstrate the results of one-bit and two-bit digitization, respectively. Finally, the performance tolerance against the bit error ratio (BER) of the coherent fiber link is also evaluated.

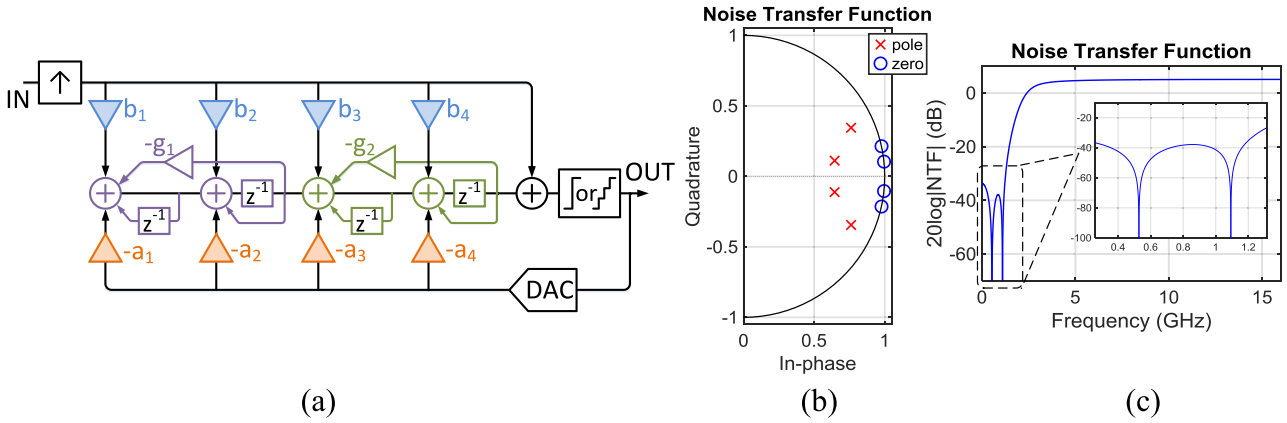

Fig. 5. Implementation of 32 GSa/s delta-sigma ADC. (a) Z-domain block diagram of a fourth-order delta-sigma ADC based on cascaded resonator feedback (CRFB) structure. (b) Zeros and poles of the noise transfer function (NTF). (c) Frequency response of the NTF.

A. *delta-sigma ADC Design*

The design of a fourth-order delta-sigma ADC based on cascaded resonator feedback (CRFB) structure is shown in Fig. 5. The Z-domain block diagram is shown in Fig. 5(a), which consists of an output quantizer, a feedback DAC, and the rest parts can be considered as a filter to the quantization noise. The transfer function of this noise filter is described by a noise transfer function (NTF), which determines the frequency distribution of quantization noise. In Fig. 5(a), there are four integrators, and every two of them, 1/(z-1) and z/(z-1), are cascaded together to form a resonator (purple and green). The number of integrators equals to the order number of the NTF. A fourth-order NTF also has two conjugate pairs (four in total) of zeroes and poles, shown in Fig. 5(b). The frequency response of the NTF is shown in Fig. 5(c).

Our design is a low-pass delta-sigma ADC where the signal is located at the low frequency end, and quantization noise is at the high frequency end. So in Fig. 5(c), the NTF is a high-pass filter, which pushes the quantization noise to the high frequency end and separates it from the signal. In the inset of Fig. 5(c), there are two notches in the stopband of the NTF, each corresponding to one pair of zeroes in Fig. 5(b). At the zeroes of NTF, quantization noise is minimized and signals at these frequency points have a maximized CNR. It should be noted that the only difference of one-bit and two-bit digitization is the quantizer at the output and the feedback DAC. Their NTFs are identical. The number of output levels is determined by the number of quantization bits. A $\log_2(\mathrm{N})$-bit quantizer outputs N levels, so one-bit quantizer outputs an OOK signal, and two-bit quantizer outputs a PAM4 signal. More details of delta-sigma ADC design can be founded in Ref [28], [29].

B. *Experimental Cases*

To evaluate the performance of delta-sigma digitization, ten experimental cases are designed, shown in Table IV. Five DOCSIS 3.1 channels are digitized by delta-sigma ADCs with sampling rates of 16, 20, 24, 28, and 32 GSa/s. Both one-bit (Case I–V) and two-bit (Case VI-X) digitization are carried out, and the five DCOSIS channels are digitized to a 16–32 Gbaud OOK (one-bit) or PAM4 (two-bit) signal, respectively. The signal baud rate after digitization is equal to the sampling rate of the ADC. In a dual-polarization coherent fiber link, each polarization has I and Q components, and each component carries one OOK/PAM4 signal, so there are four data streams in total carrying 20 digitized channels. Due to the symmetry, only 5 out of 20 DOCSIS 3.1 channels are listed in Table IV.

Unlike Nyquist ADC, whose quantization noise is evenly distributed in the Nyquist zone, delta-sigma ADC has uneven noise floor due to the noise shaping technique. In experiments, different modulations are assigned to different channels according to their CNRs, e.g., in Case V, only Ch. 2 has sufficient CNR to support 16384QAM, whereas Ch. 4 can only support 4096QAM, and the rest three can carry 8192QAM. In general, higher sampling rate leads to wider Nyquist zone, smaller in-band quantization noise, and can support higher order modulations. Two-bit digitization always has smaller quantization noise thanks to the additional bit. Therefore, in Case IX and X, all five channels have sufficient CNR to carry 16384QAM.

C. *Comparison With Nyquist ADC*

Spectral efficiency is an important figure of merit for digitization interfaces, and it is insightful to make a comparison of two digitization interfaces in terms of spectral efficiencies. Since DOCSIS 3.1 channels can support various modulations from 16QAM up to 4096QAM, the net data capacity per channel may vary dramatically; but the frequency band of five downstream DOCSIS 3.1 channels are always the same, from 258 to 1218 MHz. Therefore, to make a fair comparison, we can use the number of bits needed to digitize five DOCSIS channels as a reference.

In Table IV, for one-bit delta-sigma ADC, depending on the sampling rate, 16-32 Gb/s fiber link capacity is needed to support five digitized channels. For Case V (32 GSa/s), all five channels can support at least 4096QAM, within which at least three of them can support 8192QAM and one can carry up to 16384QAM. For two-bit ADC, the required bit number doubles. On the other hand, consider the Nyquist ADC defined in

TABLE IV
EXPERIMENTAL DESIGN OF ONE-BIT AND TWO-BIT DELTA-SIGMA DIGITIZATION

Case	Sampling rate (GSa/s) / baud rate (Gbaud)	Quantization	Waveform after ADC	Coherent transmission	Modulation formats of 5 DOCSIS channels					BER
I	16	One-bit	OOK	QPSK	128	1024	128	128	128	Error free
II	20				256	2048	256	256	256	
III	24				1024	8192	1024	1024	1024	
IV	28				2048	16384	2048	2048	2048	
V	32				8192	16384	8192	4096	8192	
VI	16	Two-bit	PAM4	16QAM	512	4096	512	512	512	
VII	20				2048	16384	2048	2048	2048	
VIII	24				4096	16384	4096	4096	4096	1.2×10^{-5}
IX	28				16384	16384	16384	16384	16384	2.8×10^{-5}
X	32				16384	16384	16384	16384	16384	1.1×10^{-4}

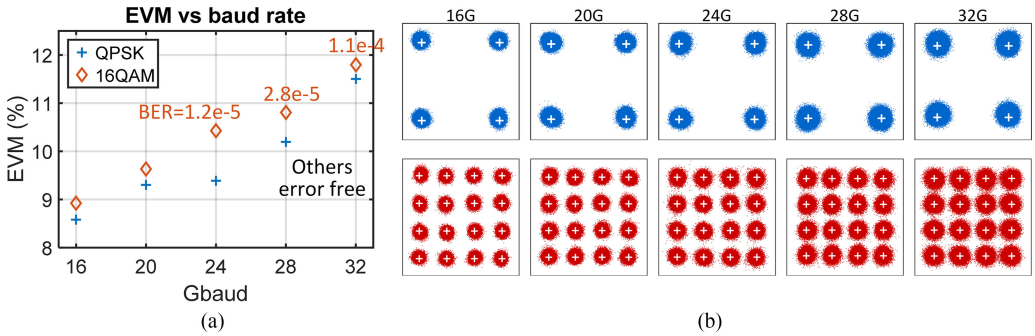

Fig. 6. Coherent transmission results of low-cost DP-QPSK and DP-16QAM systems, for one-bit and two-bit digitization, respectively. (a) Error vector magnitude (EVM) versus baud rate. (b) Constellations of QPSK and 16QAM at each baud rate.

BDR/BDF with 2.5 oversampling ratio and 12 quantization bits, it requires $1218 * 2.5$ MSa/s $* 12$ b/Sa $= 36.54$ Gb/s to digitize five DOCSIS channels.

Compared with the Nyquist ADC, one-bit delta-sigma ADC can save at least 12.4% (Case V) fiber link capacity. If CNR requirements can be relaxed, and lower sampling rate are allowed, it can save up to 56.2% (Case I) fiber link capacity. For two-bit delta-sigma ADC, although it provides much higher CNR, it generates more bits after digitization and consumes more fiber link capacity than the Nyquist ADC. It should be pointed out that the main advantage of applying delta-sigma digitization in HFC networks is to simplify fiber node design by replacing the conventional DAC with a low-cost passive filter. Improvement of spectral efficiency is a side effect.

V. EXPERIMENTAL RESULTS

In this section, we first demonstrate the experimental results of DP-QPSK and DP-16QAM coherent transmission, and then discuss the results of one-bit and two-bit digitization supported by QPSK/16QAM, respectively. Finally we will investigate the BER tolerance of delta-sigma digitization.

A. Coherent Transmission

Fig. 6 shows the results of coherent transmission of DP-QPSK/16QAM, where error vector magnitude (EVM) is plotted as a function of baud rate. Due to the limited bandwidth of low-cost RF amplifiers and the optical IQ MZM, EVM increases with baud rate. Fig. 6(b) shows the constellations at each baud rate. For DP-QPSK, error free transmission can be achieved for all baud rates. For DP-16QAM, error free transmission is only achievable for 16 and 20 Gbaud. BER values for 24, 28 and 32 Gbaud are labeled in Fig. 6(a). In the following discussion, we only present the results of 32 GSa/s delta-sigma digitization. Results of other sampling rates are similar, and omitted here for brevity.

B. One-Bit Digitization

Fig. 7 shows the experimental results of 32 GSa/s one-bit digitization (Case V). 20 DOCSIS 3.1 channels are digitized into four 32 Gb/s OOK signals, and then transmitted by a 32 Gbaud DP-QPSK link. The RF spectra before (blue) and after (red) delta-sigma digitization are shown in Fig. 7(a). Five 192-MHz DOCSIS 3.1 channels occupy a frequency range from 258 to 1218 MHz. It can be seen that after delta-sigma digitization, the signal spectrum is kept intact, and the quantization noise is pushed out of the signal band with in-band CNR larger than 40 dB. Fig. 7(b) shows the MER performance of five channels, and each of them satisfies the requirements (dashed lines) of DOCSIS 3.1 specifications. Channel 2 has MER $>$ 50 dB carrying 16384QAM; channel 4 has MER $>$ 41 dB carrying 4096QAM; the rest three channels have MER $>$ 44 (44.5) dB carrying 8192QAM. This is the first time that modulation orders higher than 4096QAM have been demonstrated over fiber in HFC networks. Constellations of each modulation are shown

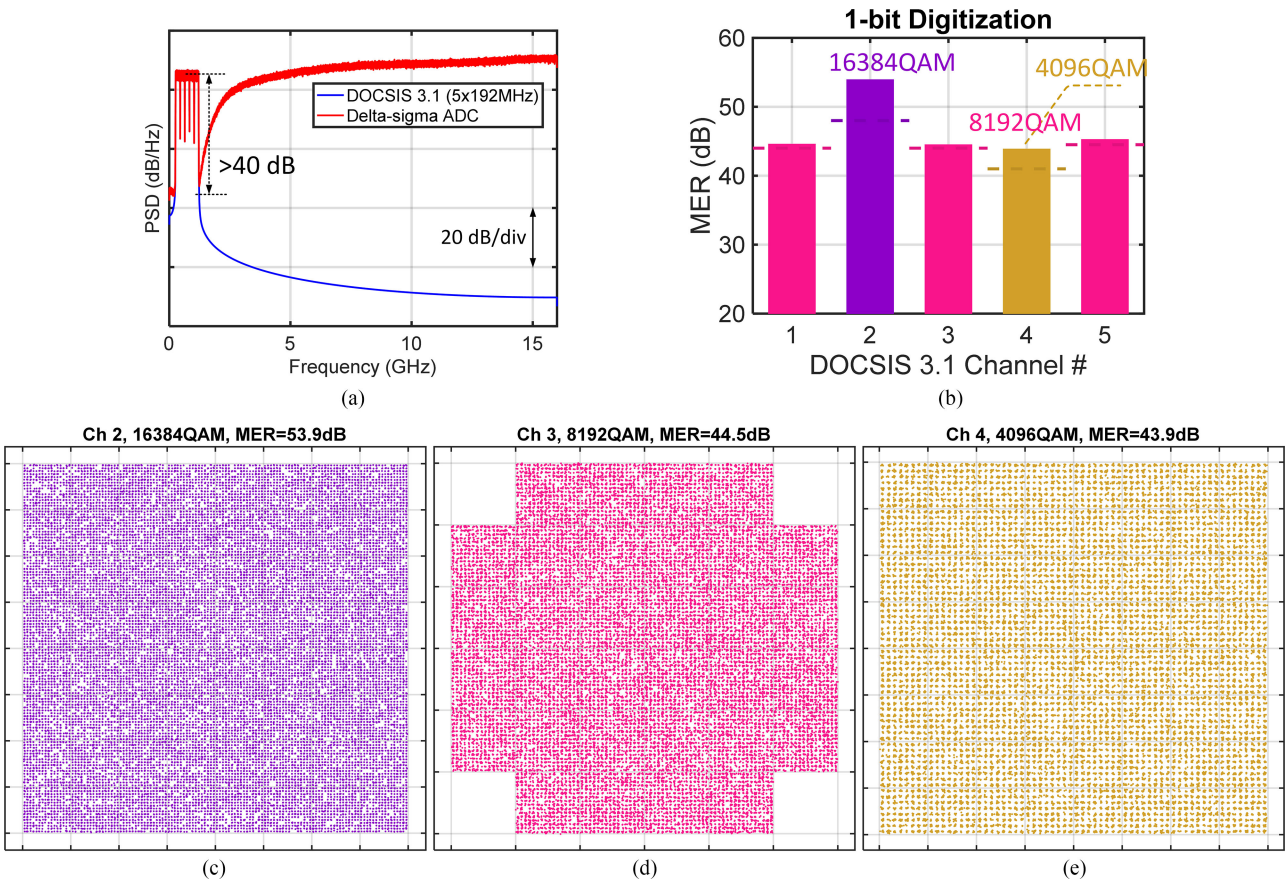

Fig. 7. Experimental results of 32 GSa/s one-bit delta-sigma digitization (Case V). (a) RF spectra before (blue) and after (red) delta-sigma digitization. (b) MER performance of five DOCSIS 3.1 channels, one carrying 16384QAM, one carrying 4096QAM, the rest three carrying 8192QAM. (c) 16384QAM constellation of channel 2. (d) 8192QAM constellation of channel 3 (worst case of 8192QAM). (e) 4096QAM constellation of channel 4.

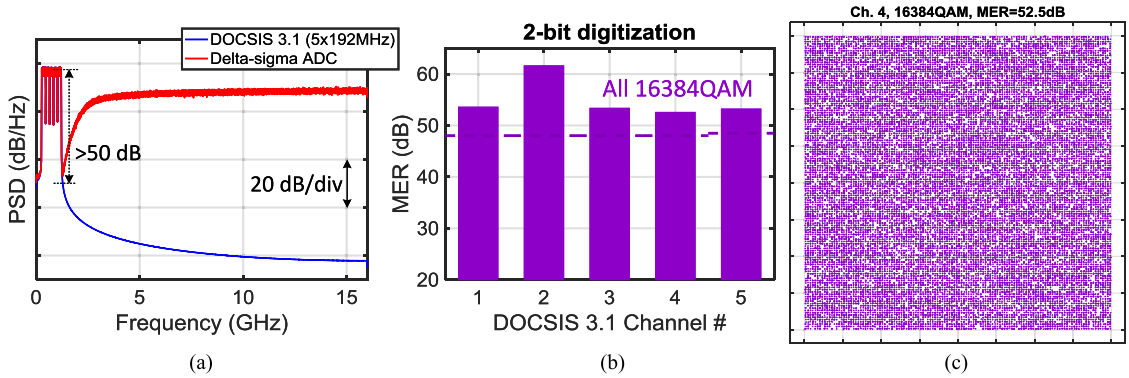

Fig. 8. Experimental results of 32 GSa/s two-bit delta-sigma digitization (Case X). (a) RF spectra before (blue) and after (red) delta-sigma digitization. (b) MER performance of five DOCSIS 3.1 channels, all carrying 16384QAM. (c) 16384QAM constellation of channel 4 (worst case).

in Fig. 7(c)–(e). For 8192QAM, the worst case of channel 3 with the lowest MER of 44.5 dB is shown in Fig. 7(d).

C. Two-Bit Digitization

Fig. 8 shows the experimental results of 32 GSa/s two-bit delta-sigma digitization (Case X). Five DOCSIS 3.1 channels are digitized into a 32 Gb/s PAM4 signal. The RF spectra before (blue) and after (red) digitization are shown in Fig. 8(a). Compared with Fig. 7(a), the in-band quantization noise is reduced thanks to the additional quantization bit, and CNR $>$ 50 dB is achieved. In Case IX and X, with sampling rates of 28 and 32 GSa/s, all 20 DOCSIS 3.1 channels have enough CNR to support 16384QAM. The raw data rate of these 20 channels is 53.2 Gb/s, and the net user information is $\sim$45 Gb/s. Since the minimum data capacity of a coherent fiber link to support 20 16384QAM channels is $28 \times 4 \times 2 = 224$ Gb/ s, the net information ratio of delta-sigma digitization is $45/224 = 20.1\%$,

TABLE V
EXPERIMENTAL DESIGN OF BER TOLERANCE EVALUATION

Case	Sampling rate (GSa/s) / baud rate (Gbaud)	Quantization	Waveform after ADC	Coherent transmission	Modulation formats of 5 DOCSIS channels				
XI	32	One-bit	OOK	QPSK	4096	4096	4096	4096	4096
XII	32	Two-bit	PAM4	16QAM	4096	4096	4096	4096	4096

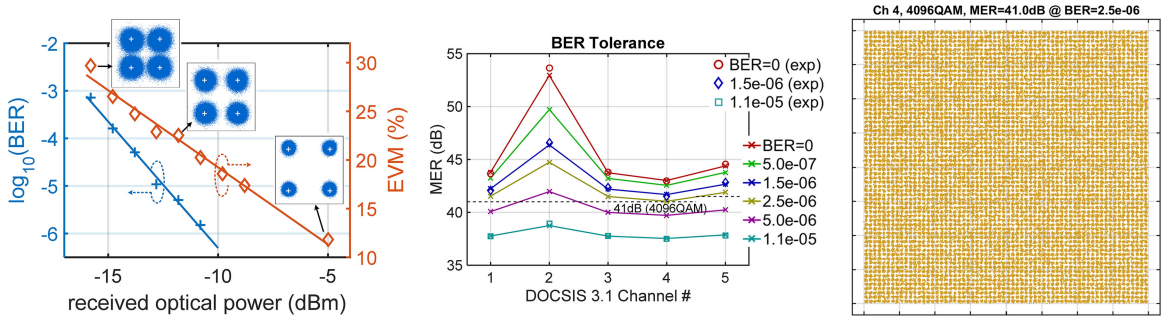

Fig. 9. BER tolerance of 32 GSa/s one-bit delta-sigma digitization. (a) BER and EVM of 32-Gbaud DP-QPSK versus received optical power. (b) MER degradation as BER increases. To satisfy the requirement of MER>41 (41.5) dB for 4096QAM, BER threshold is 2.5×10^{-6}. (c) 4096QAM constellation at the BER threshold.

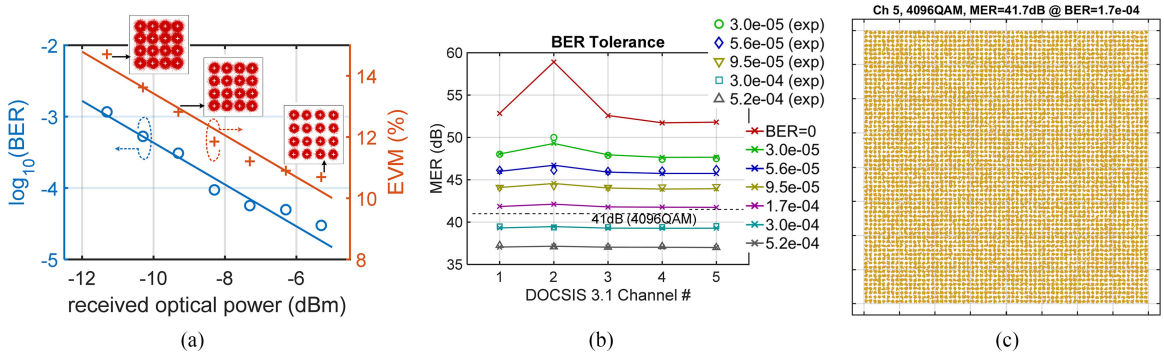

Fig. 10. BER tolerance of 32 GSa/s two-bit delta-sigma digitization. (a) BER and EVM of 32-Gbaud DP-16QAM versus received optical power. (b) MER degradation as BER increases. Thanks to the additional quantization bit, BER threshold is increased to 1.7×10^{-4}. (c) 4096QAM constellation at the BER threshold.

which is higher than the BDF/BDR interface based on Nyquist digitization. Fig. 8(b) shows the MER performance of 5 out of 20 DOCSIS channels, each with a MER larger than 52.5 dB, which is 4.5 dB higher than the required 48 dB for 16384QAM in DOCSIS 3.1 specifications. This indicates that two-bit digitization at 32 GSa/s has the potential to support even higher modulations. Fig. 8(c) shows the worst case constellation of 16384QAM, which belongs to channel 4 with the lowest MER of 52.5 dB.

D. BER Tolerance

In Table IV and Fig. 6, error free transmission is achieved for all baud rate DP-QPSK (Case I–V); but for DP-16QAM, error free transmission is only achieved at 16 and 20 Gbaud (Case VI, VII). In this section, we design BER tolerance test to measure the degradation of MER performance of delta-sigma digitization as a function of increasing BER, as shown by Case XI and XII in Table V, where 4096QAM are assigned to all 20 channels since it is the highest modulation specified in DOCSIS 3.1 specifications (8192/16384QAM are optional).

Fig. 9 shows the results of one-bit delta-sigma digitization (Case XI). The experimentally measured EVM and BER of 32 Gbaud DP-QPSK at different received optical power are presented in Fig. 9(a), with constellations plotted in the insets. Due to the limited memory of our AWG, the minimum measurable BER is 1×10^{-6}, and error free transmission is achieved for received optical power larger than -10 dBm. Fig. 9(b) shows the MER degradation as a function of the increasing BER. Both simulation (solid lines) and experiments (dots) are carried out. In the simulation, various BER values are emulated by flipping a certain amount of bits after delta-sigma digitization; whereas in the experiments, different BER values are obtained by reducing the received optical power. In experiments, it is impossible to achieve the exact BER by adjusting optical power, so in Fig. 9(b), only three values of 0, 1.5×10^{-6}, and 1.1×10^{-5}

are tested, and good consistency is achieved between simulation and experimental results. As BER increases to 2.5×10^{-6}, MER of channel 4 (worst case) drops to 41 dB, i.e., the minimum CNR requirement of 4096QAM. Therefore, the BER threshold of 32 GSa/s one-bit digitization is 2.5×10^{-6}. For $\mathrm{BER} < 2.5 \times 10^{-6}$, all 20 channels have sufficient CNR to support 4096QAM, but for BERs beyond the threshold, some channels' performance will drop below the DOCSIS 3.1 criteria. Fig. 9(c) shows the 4096QAM constellation at the BER threshold.

Similar results for two-bit delta-sigma digitization (Case XII) are shown in Fig. 10. The experimentally measured EVM and BER of 32 Gbaud DP-16QAM are shown in Fig. 10(a), and the minimum achievable BER is 3×10^{-5}. Fig. 10(b) shows the MER performance degradation as a function of the increasing BER. Simulation results (solid lines) are obtained by flipping a certain amount of bits after digitization to emulate various BER values; experimental results (dots) at $\mathrm{BER} = 3 \times 10^{-5}$, 5.6×10^{-5}, 9.5×10^{-5}, 3×10^{-4}, 5.2×10^{-4} are obtained by adjusting the received optical power. Thanks to the additional quantization bits, two-bit digitization has improved tolerance against BER. Its MER performance becomes more resilient against BER, with BER threshold increased to 1.7×10^{-4}. The 4096QAM constellation at the threshold BER is shown in Fig. 10(c).

VI. Conclusion

In this paper, we proposed and demonstrated delta-sigma digitization and coherent transmission of DOCSIS 3.1 signals for the first time. A low-pass CRFB delta-sigma ADC was designed to digitize 20×192-MHz DOCSIS 3.1 channels with 16384QAM, and transmit the digitized bits over 80-km of fiber via a single-λ 128-Gb/s DP-QPSK or 256-Gb/s DP-16QAM coherent fiber link. Both one-bit and two-bit digitization were realized and supported by QPSK and 16QAM coherent links, respectively. To facilitate its application in HFC networks, a low-cost coherent fiber system was built based on narrowband optical modulator and RF amplifiers. Frequency pre-equalization was exploited to compensate the bandwidth limitation. MER larger than 50 dB was achieved for all 20 DOCSIS 3.1 channels, and high order modulation up to 16384QAM was supported. To date, this is the highest order of modulation transmitted over fiber in HFC networks. BER tolerance of delta-sigma digitization was also evaluated and negligible degradation of MER performance was observed for BER values up to 1.5×10^{-6} and 1.7×10^{-4}, for one-bit and two-bit digitization, respectively.

References

[1] G. Kramer and G. Pesavento, "Ethernet passive optical network (EPON): Building a next-generation optical access network," *IEEE Commun. Mag.*, vol. 40, no. 2, pp. 66–73, Feb. 2002.

[2] S.-J. Park, C.-H. Lee, K.-T. Jeong, H.-J. Park, J.-G. Ahn, and K.-H. Song, "Fiber-to-the-home services based on wavelength-division-multiplexing passive optical network," *J. Lightw. Technol.*, vol. 22, no. 11, pp. 2582–2591, Nov. 2004.

[3] Y. Luo *et al.*, "Time- and wavelength-division multiplexed passive optical network (TWDM-PON) for next-generation PON stage 2 (NG-PON2)," *J. Lightw. Technol.*, vol. 31, no. 4, pp. 587–593, Feb. 2013.

[4] China Mobile, "C-RAN the road towards green RAN (version 2.5)," White Paper, Oct. 2011.

[5] A. Checko *et al.*, "Cloud RAN for mobile networks—A technology overview," *IEEE Commun. Surveys Tuts.*, vol. 17, no. 1, pp. 405–426, First Quarter 2015.

[6] T. Pfeiffer, "Next generation mobile fronthaul and midhaul architectures," *IEEE/OSA J. Opt. Commun. Netw.*, vol. 7, no. 11, pp. B38–B45, Nov. 2015.

[7] A. Pizzinat, P. Chanclou, F. Saliou, and T. Diallo, "Things you should know about fronthaul," *J. Lightw. Technol.*, vol. 33, no. 5, pp. 1077–1083, Mar. 2015.

[8] M. Toy, *Cable Networks, Services, and Management, IEEE Press Series on Networks and Services Management*. New York, NY, USA: Wiley, 2015, ch. 1.

[9] Ovum report, "HFC: Delivering Gigabit Broadband," 2016. [Online]. Available: http://www.nbnco.com.au/content/dam/nbnco2/documents/HFC%20Delivering%20Gigabit%20Broadband%20Ovum%20Report.pdf

[10] B. Hamzeh, M. Toy, Y. Fu, and J. Martin, "DOCSIS 3.1: Scaling broadband cable to Gigabit speeds," *IEEE Commun. Mag.*, vol. 53, no. 3, pp. 108–113, Mar. 2015.

[11] M. Toy, J. Martin, M. Schmitt, and V. Blake, "Next generation cable networks with DOCSIS 3.1 technology," *IEEE Commun. Mag.*, vol. 53, no. 3, pp. 106–107, Mar. 2015.

[12] H. Mehmood, S. Rahman, and J. M. Cioffi, "Bit loading profiles for high-speed data in DOCSIS 3.1," *IEEE Commun. Mag.*, vol. 53, no. 3, pp. 114–120, Mar. 2015.

[13] D. Rice, "DOCSIS 3.1 technology and hybrid fiber coax for multi-Gbps broadband," in *Proc. Opt. Fiber Commun. Conf.*, 2015, Paper Th4B.1.

[14] H. Salib, "FTTU: MSO perspective," in *Proc. Opt. Fiber Commun. Conf.*, 2016, Paper Th1I.1.

[15] *Data-Over-Cable Service Interface Specifications, DOCSIS 3.1, Physical Layer Specification, CM-SP-PHYv3.1-I09-160602*, Cable Television Laboratories, Inc., Louisville, CO, USA, Jun. 2016.

[16] *DOCSIS 3.1 Physical & MAC Layer Quick Reference Pocket Guide*," Cable Television Laboratories, Inc., Louisville, CO, USA, Sep. 2014.

[17] K. Sundaresan, *DOCSIS 3.1 High Level Overview at NANOG 59*, Cable Television Laboratories, Inc., Louisville, CO, USA, 2013. [Online]. Available: https://www.nanog.org/sites/default/files/wed.general.sundaresan.docsis.35.pdf

[18] A. Al-Banna and T. Cloonan, "The spectral efficiency of DOCSIS 3.1 systems," Arris white paper, 2014. [Online]. Available: https://www.arris.com/globalassets/resources/white-papers/arris_spectral_efficiency_of_docsis_wp.pdf

[19] H. Ibl and C. Klaus, "DOCSIS 3.1 application note," Rohde Schwarz white paper, 7MH89_0E, 2015. [Online]. Available: http://www.rohde-schwarz-usa.com/rs/rohdeschwarz/images/7mh89_oe-docsis3.1.pdf

[20] *Evolved Universal Terrestrial Radio Access (E-UTRA); Carrier Aggregation; Base Station (BS) Radio Transmission and Reception, Release 10*, 3GPP TR 36.808, V10.1.0, Jul. 2013.

[21] *New WI Proposal: LTE Carrier Aggregation Enhancement Beyond 5 Carriers*, 3GPP RP-142286, Dec. 2014.

[22] J. Wang, C. Liu, M. Zhu, A. Yi, L. Cheng, and G. K. Chang, "Investigation of data-dependent channel cross-modulation in multiband radio-over-fiber systems," *J. Lightw. Technol.*, vol. 32, no. 10, pp. 1861–1871, May 2014.

[23] J. Wang, C. Liu, M. Zhu, M. Xu, Z. Dong, and G.-K. Chang, "Characterization and mitigation of nonlinear intermodulations in multichannel OFDM radio-over-fiber systems," in *Proc. Eur. Conf. Opt. Commun.*, 2014, Paper P.7.18.

[24] J. Wang *et al.*, "Nonlinear inter-band subcarrier intermodulations for multi-RAT OFDM wireless services in 5G heterogeneous mobile fronthaul networks," *J. Lightw. Technol.*, vol. 34, no. 17, pp. 4089–4103, Sep. 2016.

[25] *Common Public Radio Interface (CPRI), Specification V7.0 (2015-10-09)*. 2015. [Online]. Available: http://www.cpri.info/downloads/CPRI_v_7_0_2015-10-09.pdf

[26] R. Gray, "Oversampled sigma-delta modulation," *IEEE Trans. Commun.*, vol. COM-35, no. 5, pp. 481–489, May 1987.

[27] P. M. Aziz, H. V. Sorensen, and J. V. der Spiegel, "An overview of sigma-delta converters," *IEEE Signal Process. Mag.*, vol. 13, no. 1, pp. 61–84, Jan. 1996.

[28] R. Schreier and G. C. Temes, *Understanding Delta-Sigma Data Converters*. New York, NY, USA: Wiley, Nov. 2004.

[29] R. Schreier, Delta Sigma Toolbox: high-level design and simulation of delta-sigma modulators. 2016. [Online]. Available: http://www.mathworks.com/matlabcentral/fileexchange/19-delta-sigma-toolbox

[30] T. P. Hung, J. Rode, L. E. Larson, and P. M. Asbeck, "Design of H-bridge class-D power amplifiers for digital pulse modulation transmitters," *IEEE Trans. Microw. Theory Techn.*, vol. 55, no. 12, pp. 2845–2855, Dec. 2007.
[31] M. Nielsen and T. Larsen, "A transmitter architecture based on delta-sigma modulation and switch-mode power amplification," *IEEE Trans. Circuits Syst. II, Express Briefs*, vol. 54, no. 8, pp. 735–739, Aug. 2007.
[32] F. M. Ghannouchi, S. Hatami, P. Aflaki, M. Helaoui, and R. Negra, "Accurate power efficiency estimation of GHz wireless delta-sigma transmitters for different classes of switching mode power amplifiers," *IEEE Trans. Microw. Theory Techn.*, vol. 58, no. 11, pp. 2812–2819, Nov. 2010.
[33] A. Jerng and C. G. Sodini, "A wideband $\Delta\Sigma$ digital-RF modulator for high data rate transmitters," *IEEE J. Solid-State Circuits*, vol. 42, no. 8, pp. 1710–1722, Aug. 2007.
[34] A. Frappe, A. Flament, B. Stefanelli, A. Kaiser, and A. Cathelin, "An all-digital RF signal generator using high-speed $\Delta\Sigma$ modulators," *IEEE J. Solid-State Circuits*, vol. 44, no. 10, pp. 2722–2732, Oct. 2009.
[35] A. Pozsgay, T. Zounes, R. Hossain, M. Boulemnakher, V. Knopik, and S. Grange, "A fully digital 65nm CMOS transmitter for the 2.4-to-2.7GHz WiFi/WiMAX bands using 5.4 GHz $\Delta\Sigma$ RF DACs," in *Proc. IEEE Int. Solid-State Circuits Conf.*, 2008, pp. 360–361.
[36] N. V. Silva, A. S. R. Oliveira, and N. B. Carvalho, "Design and optimization of flexible and coding efficient all-digital RF transmitters," *IEEE Trans. Microw. Theory Techn.*, vol. 61, no. 1, pp. 625–632, Jan. 2013.
[37] S. Chung, R. Ma, S. Shinjo, H. Nakamizo, K. Parsons, and K. H. Teo, "Concurrent multiband digital outphasing transmitter architecture using multidimensional power coding," *IEEE Trans. Microw. Theory Techn.*, vol. 63, no. 2, pp. 598–613, Feb. 2015.
[38] J. A. Wepman, "Analog-to-digital converters and their applications in radio receivers," *IEEE Commun. Mag.*, vol. 33, no. 5, pp. 39–45, May 1995.
[39] M. R. Miller and C. S. Petrie, "A multibit sigma-delta ADC for multimode receivers," *IEEE J. Solid-State Circuits*, vol. 38, no. 3, pp. 475–482, Mar. 2003.
[40] J. Arias *et al.*, "A 32-mW 320-MHz continuous-time complex delta-sigma ADC for multi-mode wireless-LAN receivers," *IEEE J. Solid-State Circuits*, vol. 41, no. 2, pp. 339–351, Feb. 2006.
[41] C. Wu, E. Alon, and B. Nikolić, "A wideband 400 MHz-to-4 GHz direct RF-to-digital multimode $\Delta\Sigma$ receiver," *IEEE J. Solid-State Circuits*, vol. 49, no. 7, pp. 1639–1652, Jul. 2014.
[42] L. Bettini, T. Christen, T. Burger, and Q. Huang, "A reconfigurable DT $\Delta\Sigma$ modulator for multi-standard 2G/3G/4G wireless receivers," *IEEE J. Emer. Sel. Topics Circuits Syst.*, vol. 5, no. 4, pp. 525–536, Dec. 2015.
[43] K. Kitamura, S. Sasaki, Y. Matsuya, and T. Douseki, "Optical wireless digital-sound transmission system with 1-bit $\Delta\Sigma$-modulated visible light and spherical Si solar cells," *IEEE Sens. J.*, vol. 10, no. 11, pp. 1753–1758, Nov. 2010.
[44] H. Qian, J. Chen, S. Yao, Z. Yu, H. Zhang, and W. Xu, "One-bit sigma-delta modulator for nonlinear visible light communication systems," *IEEE Photon. Technol. Lett.*, vol. 27, no. 4, pp. 419–422, Feb. 2015.
[45] A. Kanno and T. Kawanishi, "Analog signal transmission by FPGA-based pseudo-delta-sigma modulator," in *Proc. IEEE Photon. Conf.*, 2015, pp. 136–137.
[46] S. Jang, G. Jo, J. Jung, B. Park, and S. Hong, "A digitized IF-over-fiber transmission based on low-pass delta-sigma modulation," *IEEE Photon. Technol. Lett.*, vol. 26, no. 24, pp. 2484–2487, Dec. 2014.
[47] L. M. Pessoa, J. S. Tavares, D. Coelho, and H. M. Salgado, "Experimental evaluation of a digitized fiber-wireless system employing sigma delta modulation," *Opt. Express*, vol. 22, no. 14, pp. 17508–17523, 2014.
[48] J. Wang *et al.*, "Delta-sigma modulation for digital mobile fronthaul enabling carrier aggregation of 32 4G-LTE/30 5G-FBMC signals in a single-λ 10-Gb/s IM-DD channel," in *Proc. Opt. Fiber Commun. Conf.*, 2016, Paper W1H.2.
[49] J. Wang *et al.*, "10-Gbaud OOK/PAM4 digital mobile fronthaul based on one-bit/two-bit delta-sigma modulation supporting carrier aggregation of 32 LTE-A signals," in *Proc. Eur. Conf. Opt. Commun.*, 2016, Paper W.4.P1.SC7.1.
[50] J. Wang *et al.*, "Digital mobile fronthaul based on delta-sigma modulation for 32 LTE carrier aggregation and FBMC signals," *IEEE/OSA J. Opt. Commun. Netw.*, vol. 9, no. 2, pp. A233–A244, Feb. 2017.
[51] J. Wang, Z. Jia, L. A. Campos, C. Knittle, and G. Chang, "Optical coherent transmission of 20x192-MHz DOCSIS 3.1 channels with 16384QAM based on delta-sigma digitization," in *Proc. Opt. Fiber Commun. Conf.*, 2017, Paper Th1K.1.
[52] *Data-Over-Cable Service Interface Specifications, DCA-MHAv2, Remote PHY Specification, CM-SP-R-PHY-I07-170524*, Cable Television Laboratories, Inc., Louisville, CO, USA, May 2017.
[53] J. D. Salinger, "Remote PHY: Why and how," CableLabs, NCTA, SCTE, Spring Technical Forum, 2014.
[54] J. T. Chapman, "Remote PHY for converged DOCSIS, video and OOB," CableLabs, NCTA, SCTE, Spring Technical Forum, 2014.
[55] J. T. Chapman, G. White, and H. Jin, "Impact of CCAP to CM distance in a remote PHY architecture," CableLabs, NCTA, SCTE, Spring Technical Forum, 2015.
[56] J. D. Salinger, "Distributed architectures and converged access network," CableLabs, NCTA, SCTE, Spring Technical Forum, 2016.
[57] C.-L. I, J. Huang, Y. Yuan, S. Ma, and R. Duan, "NGFI, the xHaul," in *Proc. IEEE Globecom Workshops*, 2015, pp. 1–6.
[58] C.-L. I, Y. Yuan, J. Huang, S. Ma, C. Cui, and R. Duan, "Rethink fronthaul for soft RAN," *IEEE Commun. Mag.*, vol. 53, no. 9, pp. 82–88, Sep. 2015.
[59] C.-L. I and J. Huang, "RAN revolution with NGFI (xHaul) for 5G," in *Proc. Opt. Fiber Commun. Conf.*, 2017, Paper W1C.7.
[60] S. S. Haykin, *Adaptive Filter Theory*. Englewood Cliffs, NJ, USA: Prentice-Hall, 2001.
[61] S. J. Savory, "Digital filters for coherent optical receivers," *Opt. Express*, vol. 16, no. 2, pp. 804–817, 2008.
[62] S. J. Savory, "Digital coherent optical receivers: Algorithms and subsystems," *IEEE J. Sel. Topics Quantum Electron.*, vol. 16, no. 5, pp. 1164–1179, Sep./Oct. 2010.
[63] D. Godard, "Self-recovering equalization and carrier tracking in two-dimensional data communication systems," *IEEE Trans. Commun.*, vol. 28, no. 11, pp. 1867–1875, Nov. 1980.
[64] K. Kikuchi, "Polarization-demultiplexing algorithm in the digital coherent receiver," in *Proc. Dig. IEEE/LEOS Summer Topical Meetings*, 2008, pp. 101–102.
[65] A. Leven, N. Kaneda, U. V. Koc, and Y. K. Chen, "Frequency estimation in intradyne reception," *IEEE Photon. Technol. Lett.*, vol. 19, no. 6, pp. 366–368, Mar. 2007.
[66] S. Hoffmann *et al.*, "Frequency and phase estimation for coherent QPSK transmission with unlocked DFB lasers," *IEEE Photon. Technol. Lett.*, vol. 20, no. 18, pp. 1569–1571, Sep. 2008.
[67] A. J. Viterbi and A. M. Viterbi, "Nonlinear estimation of PSK-modulated carrier phase with application to burst digital transmission," *IEEE Trans. Inf. Theory*, vol. IT-29, no. 4, pp. 543–551, Jul. 1983.
[68] I. Fatadin, D. Ives, and S. J. Savory, "Blind equalization and carrier phase recovery in a 16-QAM optical coherent system," *J. Lightw. Technol.*, vol. 27, no. 15, pp. 3042–3049, Aug. 2009.

Authors' biography not available at the time of publication.